Particle detection using closed-loop active model diagnosis

Noom, Jacques; Soloviev, Oleg; Smith, Carlas; Thao, Nguyen Hieu; Verhaegen, Michel

DOI
10.1117/12.2605452

Publication date
2022

Document Version
Final published version

Published in
AI and Optical Data Sciences III

Citation (APA)
Noom, J., Soloviev, O., Smith, C., Thao, N. H., & Verhaegen, M. (2022). Particle detection using closed-loop active model diagnosis. In B. Jalali, & K. Kitayama (Eds.), *AI and Optical Data Sciences III* Article 120190F (Proceedings of SPIE - The International Society for Optical Engineering; Vol. 12019). SPIE. https://doi.org/10.1117/12.2605452

PROCEEDINGS OF SPIE

SPIEDigitalLibrary.org/conference-proceedings-of-spie

Particle detection using closed-loop active model diagnosis

Noom, Jacques, Soloviev, Oleg, Smith, Carlas, Nguyen, Hieu Thao, Verhaegen, Michel

Jacques Noom, Oleg Soloviev, Carlas Smith, Hieu Thao Nguyen, Michel Verhaegen, "Particle detection using closed-loop active model diagnosis," Proc. SPIE 12019, AI and Optical Data Sciences III, 120190F (2 March 2022); doi: 10.1117/12.2605452

SPIE.

Event: SPIE OPTO, 2022, San Francisco, California, United States

Particle detection using closed-loop active model diagnosis

Jacques Noom[a], Oleg Soloviev[a], Carlas Smith[a], Nguyen Hieu Thao[a], and Michel Verhaegen[a]

[a]Delft Center for Systems and Control, Delft University of Technology, Mekelweg 2, 2628CD Delft, The Netherlands

ABSTRACT

We demonstrate a novel closed-loop input design technique on the detection of particles in an imaging system such as a fluorescence microscope. The probability of misdiagnosis is minimized while constraining the input energy such that for instance phototoxicity is reduced. The key novelty of the closed-loop design is that each next input is designed based on the most recent information. Using updated hypothesis probabilities, the input energy distribution is optimized for detection such that unresolved pixels have increased illumination next image acquisition. As compared to conventional open-loop, the results show that (regions of) particles are diagnosed using less energy in the closed-loop approach. Besides the closed-loop approach being viable for particle detection in fluorescence microscopy measurements, it can be developed further to apply in different areas such as sequential object segmentation for reliable and efficient product inspection in Industry 4.0.

Keywords: Active fault diagnosis, Auxiliary signal design, Fluorescence microscopy, Machine vision

1. INTRODUCTION

Superresolution microscopy aims at nanometer-precision localization of single particles. A major limitation is the photon budget per emitter. MINFLUX[1] is a recently developed method for accurate estimation of particle locations, while using the photon budget efficiently. However, the particles first need to be detected before the MINFLUX procedure can be started. Previous efforts[2,3] detect particles with uniform illumination and only using a single shot (e.g. coarse xy-scanning for only a single time). Clearly, this provides opportunities for improvement in reducing the photodamage to the tissue, and thereby potentially enhancing the localization precision.

Closed-Loop Active Model Diagnosis (CLAMD) discriminates models in the fewest number of measurements by sequentially applying the online calculated separating input to the system. It stems from active fault diagnosis[4] and auxiliary signal design,[5] in which auxiliary inputs are designed to verify whether a system is faulty or not. Active fault diagnosis "has not seen widespread adoption in practical applications."[4] However, the theory developed under this name is considerably more general than diagnosing *faults*. It is rather concerned with diagnosing *models*, which is also associated with, for example, pattern recognition and the detection of particles under a microscope. Therefore, in accordance with recent literature,[6] this paper is continued with the term *'model diagnosis'*.

The efforts mentioned earlier[2,3] using one single measurement are examples of *open-loop* active model diagnosis. They are active for having a controllable, yet predefined (in this case uniform) input illumination. Also the techniques using sequential measurements, as in sequential analysis,[7] with a predefined input are still categorized under open-loop. The *closed-loop* aspect is introduced when the next discriminating input is designed based on most recent information, as early[5,8,9] and more recent contributions[4] propose. This is likely to be more appropriate for quick and efficient diagnosis.

After the contribution with application to automated visual inspection,[6] this paper further stimulates research in CLAMD by showing how it can be applied to particle detection. Challenging realistic conditions under a fluorescence microscope are simulated, after which the closed-loop procedure finds the particle locations. Its performance is then compared to that of an open-loop approach. Additionally, the methodology is tested on a situation where neighboring pixels are not independent due to the large size of the point-spread function (PSF).

E-mail: j.noom@tudelft.nl

AI and Optical Data Sciences III, edited by Bahram Jalali, Ken-ichi Kitayama, Proc. of SPIE Vol. 12019, 120190F
© 2022 SPIE · 0277-786X · doi: 10.1117/12.2605452

2. METHODS

Consider the object to be imaged $x \in \{0,1\}^{m\times m}$. For each element $i \in \{1,2,\ldots,m^2\}$, two hypotheses are formulated whether it contains a particle or not:

$$\begin{aligned} M_0 &: x_i = 0 \\ M_1 &: x_i = 1. \end{aligned} \tag{1}$$

The mathematical model for the image formation is

$$y_k = h_x * \big(x \cdot (h_u * u_k)\big) + v_k, \tag{2}$$

with $u_k \in \mathbb{R}_+^{m\times m}$ the illumination input, $y_k \in \mathbb{R}_+^{m\times m}$ the output intensity, $h_x, h_u \in \mathbb{R}_+^{m\times m}$ the point-spread function (PSF) of the imaging system and illumination source, respectively, and $v_k \in \mathbb{R}^{m\times m}$ the noise at measurement k. The symbols $*$ and $\cdot$ represent convolution and element-wise multiplication, respectively.

With the statistics of the stochastic variable v_k known, the hypothesis probabilities $P_{i,k}(M_j)$ evolve according to the Bayesian update rule

$$P_{i,k}(M_j) = \frac{p(y_{i,k}|M_j)P_{i,k-1}(M_j)}{p(y_{i,k})}, \tag{3}$$

where $p(y_{i,k}|M_j)$ is the probability density function (PDF) of output y_k at pixel* i, conditioned on hypothesis M_j. The initial conditions $P_{i,0}(M_j)$ can be set to any prior probabilities. Note that the PDFs are taken here independent of neighboring pixels. This means that only the response at output pixel $y_{i,k}$ is regarded for assessing whether object element x_i contains a particle, without regarding pixels neighboring to $y_{i,k}$. Therefore, it is assumed that h_x is centered and narrow.

In the current application we limit the so-called input energy

$$\sum_i u_{i,k}^2 = \mathrm{vec}(u_k)^\top \mathrm{vec}(u_k) \leq \varepsilon. \tag{4}$$

This concept can have physical meaning and purpose, for instance for reduced phototoxicity or bleaching in fluorescence microscopy. Note that this definition of the input energy is standard in control engineering, but can be different from the physical energy in reality.

2.1 Closed-Loop Input Determination

Based on the probabilities calculated in (3), the input energy ε for next acquisition is distributed as follows:

$$u_{i,k+1} = \sqrt{\frac{P_{i,k}(M_0)P_{i,k}(M_1)}{\sum_\ell P_{\ell,k}(M_0)P_{\ell,k}(M_1)}\,\varepsilon} \tag{5}$$

This function is chosen heuristically, though with the logic that larger inputs are desirable if $P_{i,k}(M_1) = 1 - P_{i,k}(M_0) \approx 0.5$ and otherwise, smaller inputs are affordable. Note that this works only if the illumination does not have a lateral offset. This means that h_u is centered, but not necessarily narrow. The diagnosis algorithm is applied in closed-loop, as illustrated in Figure 1. The imaging system performs operation (2) and the controller computes both (3) and (5).

3. SIMULATION RESULTS

In this section, first the results are shown for a Monte-Carlo simulation where the PSF is small compared to the pixel size. Afterwards, the effect of a larger PSF is evaluated. For both experiments, the acquired images have size 50×50 pixels and consist of 15 randomly distributed particles. This makes the initial probability for each pixel $P_{i,0}(M_1) = 15/2500$. The input characteristic h_u is a centered Gaussian with standard deviation 2 pixels. The open-loop approach applies uniform illumination over a number of measurements equivalent to the closed-loop approach. We consider two cases of the output PSF h_x: sharp and wide.

*The notation for individual elements i in $m \times m$-matrices is in this paper indicated as first subindex, e.g.: $u_{i,k}$ for matrix u_k, or $P_{i,k}(M_j)$ for matrix $P_k(M_j)$.

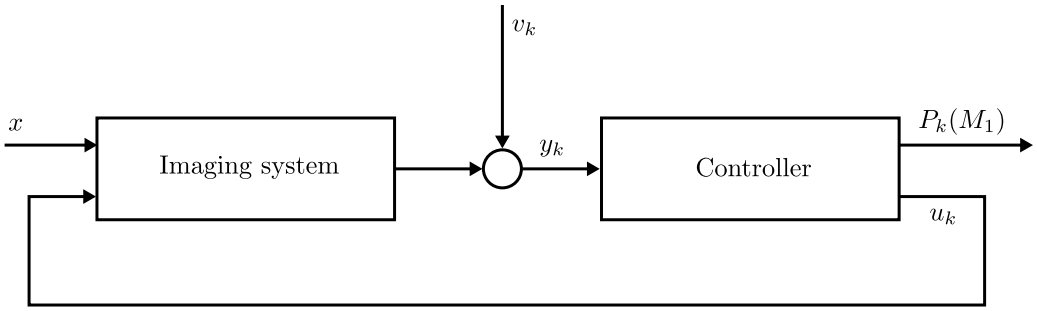

Figure 1. Control scheme. The (unknown) object x is fed to the imaging system together with illumination input u_k. Its output is corrupted with noise v_k, after which y_k is measured. The controller determines the probabilities of particle presence for each pixel $P_k(M_1)$ and computes the input for next measurement.

3.1 Sharp PSF

The imaging system in this experiment is assumed to have a small PSF compared to the pixel size. This implies that each photon emitted from object element x_i will be received only in output element $y_{i,k}$ and not in neighboring pixels. The images are corrupted with Poisson noise with 20 photons background noise and the input energy is $\varepsilon = 10^5$ squared photons[†], which implies that two photons per emitter can be expected per measurement if the sample is uniformly illuminated. The maximum number of measurements is 200 and 800 Monte-Carlo runs are performed.

Video 1 shows the precision and recall[‡] characteristics resulting from the Monte-Carlo runs, together with one realization of the particle probabilities and corresponding input (paused at time step $k = 90$). From the precision-recall curves and the corresponding area under the curve, it can be clearly seen that the closed-loop approach converges faster to the ground truth. The reason for this is that the closed-loop approach inspects unresolved areas with higher illumination intensity than areas with higher confidence. The bottom right plot reveals this effect, by showing larger inputs at areas where $P_{i,k}(M_1) \approx 0.5$. In addition, when comparing the summed input energy for all measurements until an Area Under the Curve (AUC) of 0.98 is achieved, it can be concluded that the closed-loop approach ($k = 91$) uses 27.8% less energy than the open-loop approach ($k = 126$). The illumination at the true particle locations – which is direcly related to bleaching – was reduced with 18.6% using the closed-loop approach.

3.2 Wide PSF

Now, a larger PSF of the imaging system is considered, making neighboring pixels dependent. Nevertheless, the same strategy from Section 2 is still used. The PSF h_x is modeled as a centered Gaussian with standard deviation 1.2 pixels.Then, the images are corrupted with Poisson noise with 5 photons background noise. The input energy is $\varepsilon = 62\,500$ squared photons, implying that 5 photons per emitter are expected each measurement in the case of uniform illumination.

Video 2 shows the results for one realization (paused at time step $k = 100$). At first sight, it appears that the closed-loop approach finds the particles with significantly more confidence than the open-loop approach using uniform illumination. On the other hand, for both approaches the probability plots show circular blobs with high confidence, instead of single pixels. This produces apparent rings with low confidence (i.e. $P_{i,k}(M_1) \approx 0.5$) around the actual particles. Therefore, the closed-loop approach suggests large illumination very close to the particle locations, thereby inadvertently illuminating the particles itself with a higher intensity. Nevertheless, the photodamage to the general tissue can still be decreased, as the particles are detected in fewer measurements and thus using less input energy in total, as compared to the open-loop approach using uniform illumination.

[†]As mentioned in Section 2, the definition of input energy in control engineering can be different from the physical energy in reality.

[‡]Precision is defined as TP/(TP+FP), and recall is TP/(TP+FN), with TP, FP and FN the true positives, false positives and false negatives, respectively.

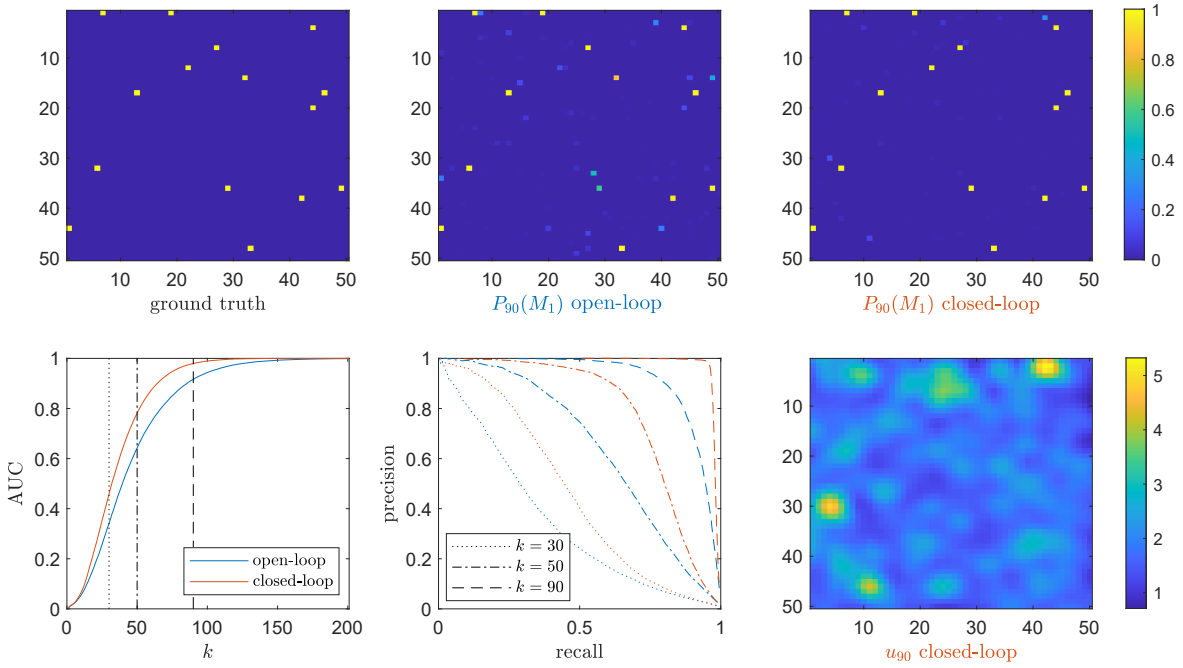

Video 1. Results of Monte-Carlo runs for small PSF. (Bottom middle) precision-recall curves for $k = \{30, 50, 90\}$ for open-loop (blue) and closed-loop approach (red). (Bottom left) the Area Under precision-recall Curve (AUC) over time. (Remaining) one realization at time step $k = 90$: ground truth (top left), particle probabilities for open-loop (top middle) and closed-loop approach (top right), and the corresponding input (bottom right). Using nonuniform closed-loop illumination, the probabilities converge faster to the ground truth. http://dx.doi.org/10.1117/12.2605452.1

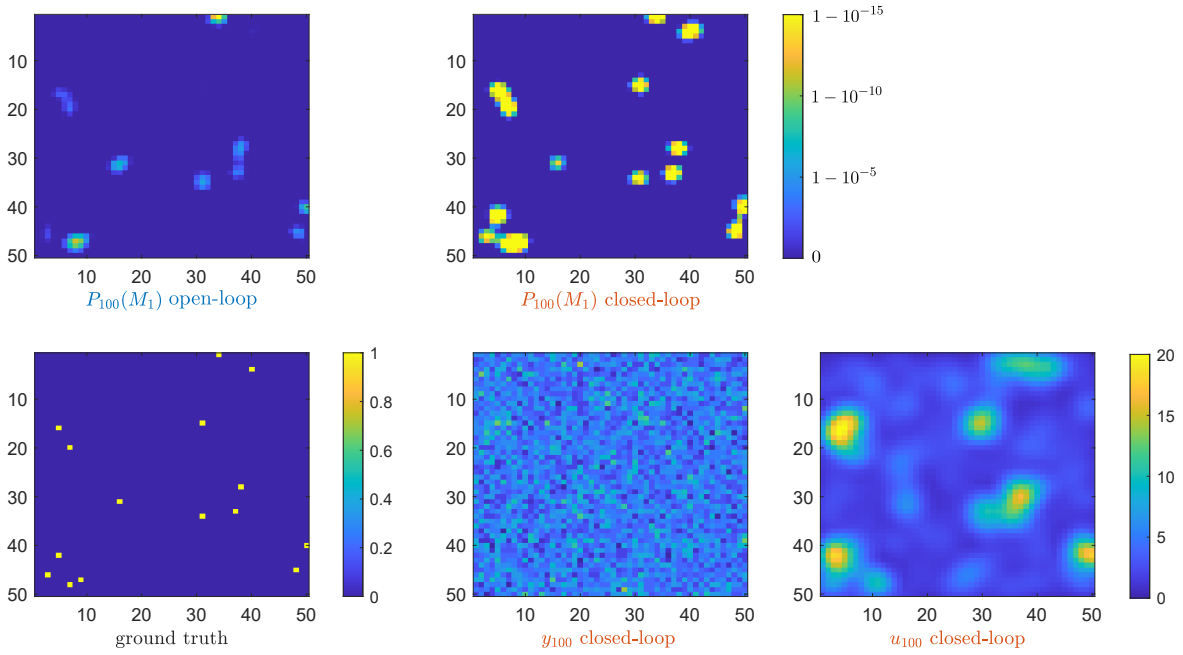

Video 2. Results of the simulation with larger PSF. The ground truth (bottom left), the particle probabilities for open-loop (top left) and closed-loop approach (top middle), the output (bottom middle) and the input (bottom right) at time step $k = 100$. Although the effect of larger PSF is clearly visible in the probability plots, it can be seen that the closed-loop approach converges faster in the direction of the ground truth. http://dx.doi.org/10.1117/12.2605452.2

If regarding the measurement number for which the average probability for the positives exceeds 98% (closed-loop: $k = 46$ with average $P_{i,46}(M_1)$ for negatives 6.7%; open-loop: $k = 119$ with average $P_{i,119}(M_1)$ for negatives 4.7%), it turns out that this specific realization uses 61.3% less energy and reduces bleaching of the emitters with 29.0% in closed-loop. Surprisingly, this means that the closed-loop approach performed better in this case, despite the degenerate behavior of focusing illumination around the actual particles. Still, there are substantial opportunities for improvement in efficient distribution of illumination intensity. To achieve that, it remains a challenge to consider dependencies between neighboring pixels.

4. CONCLUSIONS

This manuscript demonstrated the application of CLAMD to particle detection in imaging systems. By considering probabilities of particle presence in a pixel, the proposed approach calculates an illumination pattern such that the overall confidence increases, while using limited input energy. A first test under challenging conditions for a fluorescence microscope with small PSF showed a decrease in energy usage of 27.8% and in bleaching of the particles of 18.6%. An additional test with large PSF also demonstrated an improvement in performance, yet revealed the degenerate behavior of this implementation of inadvertently focusing illumination on the particles.

Further developments should focus on considering the dependency between pixels if the PSF is wide. Another recommendation is to perform the detection with (sub-pixel) localization simultaneously, instead of subsequently. This would lead to a more efficient use of the photon budget of the particles, and therefore a more accurate localization. After this demonstration in particle detection, the applicability of CLAMD can be expanded to detecting extended objects with limited input energy, which could be useful in reliable and efficient medical diagnosis or product inspection in Industry 4.0.

ACKNOWLEDGMENTS

This project has received funding from the ECSEL Joint Undertaking (JU) under grant agreement No 826589. The JU receives support from the European Union's Horizon 2020 research and innovation programme and Netherlands, Belgium, Germany, France, Italy, Austria, Hungary, Romania, Sweden and Israel.

REFERENCES

[1] Balzarotti, F., Eilers, Y., Gwosch, K. C., Gynnå, A. H., Westphal, V., Stefani, F. D., Elf, J., and Hell, S. W., "Nanometer resolution imaging and tracking of fluorescent molecules with minimal photon fluxes," *Science* **355**(6325), 606–612 (2017).

[2] Gwosch, K. C., Pape, J. K., Balzarotti, F., Hoess, P., Ellenberg, J., Ries, J., and Hell, S. W., "MINFLUX nanoscopy delivers 3D multicolor nanometer resolution in cells," *Nature Methods* **17**, 217–224 (2020).

[3] Smith, C. S., Stallinga, S., Lidke, K. A., Rieger, B., and Grunwald, D., "Probability-based particle detection that enables threshold-free and robust in vivo single-molecule tracking," *Molecular Biology of the Cell* **26**(22), 4057–4062 (2015).

[4] Heirung, T. A. N. and Mesbah, A., "Input design for active fault diagnosis," *Annual Reviews in Control* **47**, 35–50 (2019).

[5] Zhang, X. J. and Zarrop, M. B., "Auxiliary signals for improving on-line fault detection," in [*1988 International Conference on Control - CONTROL 88*], 414–419 (1988).

[6] Noom, J., Thao, N. H., Soloviev, O., and Verhaegen, M., "Closed-Loop Active Model Diagnosis Using Bhattacharyya Coefficient: Application to Automated Visual Inspection," in [*Intelligent Systems Design and Applications (ISDA 2020)*], Abraham, A., Piuri, V., Gandhi, N., Siarry, P., Kaklauskas, A., and Madureira, A., eds., 657–667, Springer, Cham (2021).

[7] Wald, A., [*Sequential Analysis*], John Wiley & Sons, Inc., New York (1947).

[8] Hunter, W. G. and Reiner, A. M., "Designs for Discriminating Between Two Rival Models," *Technometrics* **7**(3), 307–323 (1965).

[9] Box, G. E. and Hill, W. J., "Discrimination Among Mechanistic Models," *Technometrics* **9**(1), 57–71 (1967).